SPITZER OBSERVATIONS OF MF 16 NEBULA AND THE ASSOCIATED ULTRALUMINOUS X-RAY SOURCE

C. T. Berghea and R. P. Dudik

United States Naval Observatory, Washington, DC 20392, USA; ciprian.berghea@usno.navy.mil, rpdudik@usno.navy.mil

ABSTRACT

We present *Spitzer* Infrared Spectrograph observations of the ultraluminous X-ray source (ULX) NGC 6946 X-1 and its associated nebula MF 16. This ULX has very similar properties to the famous Holmberg II ULX, the first ULX to show a prominent infrared [O IV] emission line comparable to those found in active galactic nuclei. This paper attempts to constrain the ULX spectral energy distribution (SED) given the optical/UV photometric fluxes and high-resolution X-ray observations. Specifically, *Chandra* X-ray data and published *Hubble* optical/UV data are extrapolated to produce a model for the full optical to X-ray SED. The photoionization modeling of the IR lines and ratios is then used to test different accretion spectral models. While either an irradiated disk model or an O-supergiant plus accretion disk model fits the data very well, we prefer the latter because it fits the nebular parameters slightly better. In this second case the accretion disk alone dominates the extreme-UV and X-ray emission, while an O-supergiant is responsible for most of the far-UV emission.

Key words: black hole physics – galaxies: individual (NGC 6946)– infrared: ISM – X-rays: binaries

1. INTRODUCTION

The suggestion that ultraluminous X-ray sources (ULXs) in nearby galaxies may harbor intermediate-mass black holes (IMBHs; e.g., Colbert & Mushotzky 1999) has major implications on the studies of black hole (BH) formation and evolution. However, the evidence for this new type of BH has been slow to accumulate. Other explanations have been proposed to account for the high X-ray luminosities of ULXs, such as super-Eddington accretion (Done & Kubota 2006; Kuncic et al. 2007; King 2008; Soria & Kuncic 2008; Berghea et al. 2008; Abolmasov 2011) or beaming (Körding et al. 2002; King 2008). Some galactic binaries are known to show super-Eddington luminosities, such as GRS 1915+105 (Fender & Belloni 2004) and V4641 Sgr (Revnivtsev et al. 2002). However, conclusive evidence on the true nature of some or all known extragalactic ULXs has remained elusive.

One of the most interesting developments in ULX history is the discovery in recent years of large ionized bubble nebulae around some of the most famous ULXs (Pakull & Mirioni 2002). These are much larger and more luminous than regular supernova remnants (SNRs). In addition, high-ionization lines have been detected, such as He II $\lambda4686$ (I.P. = 54.4 eV; e.g., Abolmasov et al. 2007; Moon et al. 2011). Kaaret & Corbel (2009) detected [Ne v] $\lambda3426$ from the nebula associated with the ULX in NGC 5408 (I.P. = 97.1 eV). The detection of these lines suggests photoionization of the surrounding gas by the hard radiation from the accreting ULX, similar to what happens with active galactic nuclei (AGNs).

It is also remarkable that there may exist such an object in our own Galaxy. The first recognized microquasar, the famous SS 433 (Stephenson & Sanduleak 1977) is possibly the "closest" relative to the nebula-surrounded ULXs. It is surrounded by a 100 pc radio nebula, W 50 (Dubner et al. 1998) and is most likely super-Eddington (e.g., Fabrika 2004). Indeed, SS 433 could be an example of both beaming *and* super-Eddington accretion, the combination of which could easily explain even the most luminous ULXs (Begelman et al. 2006; Poutanen et al. 2007). It is seen almost edge-on and therefore most of its strong UV and X-ray radiation is likely not visible. However, if such objects exist in nearby galaxies, those seen at small inclination angles

should appear as bright ULXs. Recently, an object very similar to SS 433 was discovered in the galaxy NGC 7793 (Pakull et al. 2010; Soria et al. 2010), showing radio lobes and hot spots, like a bona-fide quasar.

Vázquez et al. (2007) conducted the first infrared spectroscopy study of ULXs. They obtained high-resolution *Spitzer* spectra of six ULXs in NGC 4485/90. Vázquez et al. (2007) looked for the mid-infrared [O IV] high-ionization line, which has an equivalent ionization potential to He II. However, apart from a possible weak detection in one object in their sample (ULX-1, which is probably an SNR), [O IV] was not found in the NGC 4485/90 ULXs.

The first reliable detection of [O IV] associated with an ULX was the famous Holmberg II ULX (Berghea et al. 2010a, 2010b). It is also one of the most interesting examples of an ionized nebula associated with a ULX (Pakull & Mirioni 2002; Lehmann et al. 2005; Abolmasov et al. 2007). He II is detected in a small nebular region around the ULX, the "Heel" of the "Foot Nebula" (Pakull & Mirioni 2002; Kaaret et al. 2004). An OB star is the likely counterpart. The morphology of He II emission and other optical lines is consistent with the photoionization of the nebula by the ULX (Pakull & Mirioni 2002). Kaaret et al. (2004) confirmed this using the *Hubble Space Telescope* (*HST*). Miller et al. (2005) detected extended radio emission from a ∼50 pc diameter region coincident with the position of the ULX. These authors conclude that the flux and morphology of the radio emission are inconsistent with emission from an SNR or an H II region, and is probably associated with the ULX activity. Using new observations, Cseh et al. (2012) suggest that the radio emission is probably caused by a weakly collimated outflow, rather than a jet.

The ULX that we investigate in this paper (which we will call NGC 6946 X-1 hereafter) was first identified as such by Roberts & Colbert (2003), who showed that the X-ray variability of this source indicates a binary origin. MF 16 has been known as a very luminous SNR Matonick & Fesen (1997) associated with a *ROSAT* X-ray source and a radio source (van Dyk et al. 1994). Abolmasov et al. (2008) used optical spectroscopy to conclude that the ULX is most likely responsible for the high-ionization lines detected in the MF 16 nebula. They suggest that the ULX is probably bright in UV/EUV and not only in X-rays

Report Documentation Page

1. REPORT DATE	2. REPORT TYPE	3. DATES COVERED
JUN 2012		**00-00-2012 to 00-00-2012**

4. TITLE AND SUBTITLE		5a. CONTRACT NUMBER
Spitzer Observations Of MF 16 Nebula And The Associated Ultraluminous X-Ray Source		5b. GRANT NUMBER
		5c. PROGRAM ELEMENT NUMBER
6. AUTHOR(S)		5d. PROJECT NUMBER
		5e. TASK NUMBER
		5f. WORK UNIT NUMBER

7. PERFORMING ORGANIZATION NAME(S) AND ADDRESS(ES)	8. PERFORMING ORGANIZATION REPORT NUMBER
United States Naval Observatory,Washington,DC,20392	

9. SPONSORING/MONITORING AGENCY NAME(S) AND ADDRESS(ES)	10. SPONSOR/MONITOR'S ACRONYM(S)
	11. SPONSOR/MONITOR'S REPORT NUMBER(S)

12. DISTRIBUTION/AVAILABILITY STATEMENT

Approved for public release; distribution unlimited

14. ABSTRACT

We present Spitzer Infrared Spectrograph observations of the ultraluminous X-ray source (ULX) NGC 6946 X-1 and its associated nebula MF 16. This ULX has very similar properties to the famous Holmberg II ULX, the first ULX to show a prominent infrared [O iv] emission line comparable to those found in active galactic nuclei. This paper attempts to constrain the ULX spectral energy distribution (SED) given the optical/UV photometric fluxes and high-resolution X-ray observations. Specifically, Chandra X-ray data and published Hubble optical/UV data are extrapolated to produce a model for the full optical to X-ray SED. The photoionization modeling of the IR lines and ratios is then used to test different accretion spectral models. While either an irradiated disk model or an O-supergiant plus accretion disk model fits the data very well, we prefer the latter because it fits the nebular parameters slightly better. In this second case the accretion disk alone dominates the extreme-UV and X-ray emission, while an O-supergiant is responsible for most of the far-UV emission.

15. SUBJECT TERMS

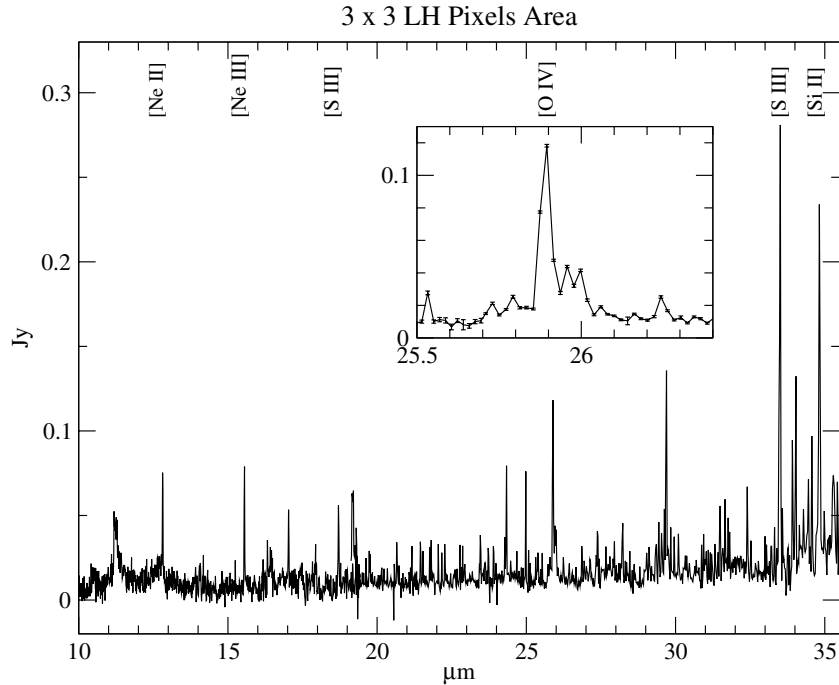| 16. SECURITY CLASSIFICATION OF:			17. LIMITATION OF ABSTRACT	18. NUMBER OF PAGES	19a. NAME OF RESPONSIBLE PERSON
a. REPORT **unclassified**	b. ABSTRACT **unclassified**	c. THIS PAGE **unclassified**	**Same as Report (SAR)**	**11**	

Figure 1. Full IRS spectra obtained from matched apertures with CUBISM from the aperture shown in Figure 2.

(predicted absorbed flux at 1000 Å: 10^{-17} erg cm^{-2} s^{-1} Å^{-1}). This was actually verified by Kaaret et al. (2010), who used the Advanced Camera for Surveys (ACS) on the *HST* to detect far-UV emission from the ULX for the first time. The data do not allow the authors to conclude with certainty what the UV source is, but they suggest it is a combination of disk emission and contribution from an OB supergiant.

Recently, a tentative quasi-periodic oscillation of $\sim$8.5 MHz was detected (Rao et al. 2010) using *XMM-Newton* X-ray data which—if confirmed—makes the NGC 6946 X-1 the fourth ULX with such timing features (two ULXs in M82 and NGC 5408 X-1). NGC 6946 X-1 is very similar to the Holmberg II ULX in many respects. Berghea et al. (2010b) used Mappings III photoionization and shock modeling to show that NGC 6946 X-1 and Holmberg II ULX high-ionization line fluxes primarily result from photoionization rather than shocks (see also Section 4.1.).

In this paper, we use IR *Spitzer* spectroscopic observations to constrain the UV and soft X-ray emission of the NGC 6946 X-1. The IR observations, when combined with previously published optical, UV, and X-ray data, suggest that the powerful UV and soft X-ray emission from NGC 6946 X-1 photoionizes the surrounding medium. In Section 2, we present the *Spitzer* Infrared Spectrograph (IRS) data analysis and *Chandra* X-ray spectral fitting results. In Section 3, we use our data and other published data to construct a spectral energy distribution (SED) of the ULX which is then used as photoionization source in CLOUDY modeling. Finally, in Section 4 we use our results to compare the ionization properties of this famous ULX with those of standard AGNs.

2. DATA PROCESSING AND RESULTS

2.1. Spitzer IRS Observations

The data presented here are archival *Spitzer* data, taken on 2009 February 21. The IRS spectral map is described by 4 parallel pointings and 12 perpendicular pointings at half-slit

steps, for the short high (SH; in the range 9.9–19.6 μm) module. The long high (LH) map (in the range 18.7–37.2 μm) has three parallel pointings and seven perpendicular pointings.

The total exposure time was 1.4 ks and 1.3 ks for SH and LH observations, respectively. The data were preprocessed by the IRS pipeline (version 18) at the Spitzer Science Center prior to download. Spectral maps were constructed using "BCD-level" processed data in conjunction with CUbe Builder for IRS Spectra Maps (CUBISM) version 1.5[1] (Smith et al. 2007; Kennicutt et al. 2003). The absolute calibration error on fluxes obtained with CUBISM is $\sim$25% (Smith et al. 2004). We adopt a distance of 5.1 Mpc to NGC 6946 as in Kaaret et al. (2010; 1″ is 25 pc). The LH maps obtained with CUBISM have intrinsic sizes of 26″.4 by 17″.6 (660 pc by 440 pc), while the SH maps are 23″ by 13″.8 (575 pc by 345 pc). However, in order to avoid aperture effects, the spectra presented here were extracted from a like-sized aperture. Thus, the SH and LH spectral data result from an equally sized square aperture of size 13″.3 (332.5 pc), which is composed of 9 LH pixels centered on the ULX position.

The high-resolution spectra (10–37 μm) are plotted in Figure 1. Since the spectra are extracted from matched apertures, the spectral lines in both the SH and LH modules are properly calibrated and the continuum is properly matched. We used Spectroscopic Modeling Analysis and Reduction Tool (SMART; see Higdon et al. 2004) version 8.1.2 to measure line fluxes. The fluxes of detected lines and upper limits for non-detections are presented in Table 1. We note that the [O IV] line is detected at a signal-to-noise ratio >12. Abolmasov et al. (2008) estimates an extinction of $A_V =1.54$ mag in the direction of NGC 6946 X-1. For the infrared lines, we estimate from Draine (1989) that the extinction is $A_\lambda < 0.1$, and therefore negligible.

The SH and LH maps for the detected lines are presented in Figure 2. They are shown together with two *HST* images of

---

[1] Available at: http://ssc.spitzer.caltech.edu/archanaly/contributed/cubism/.
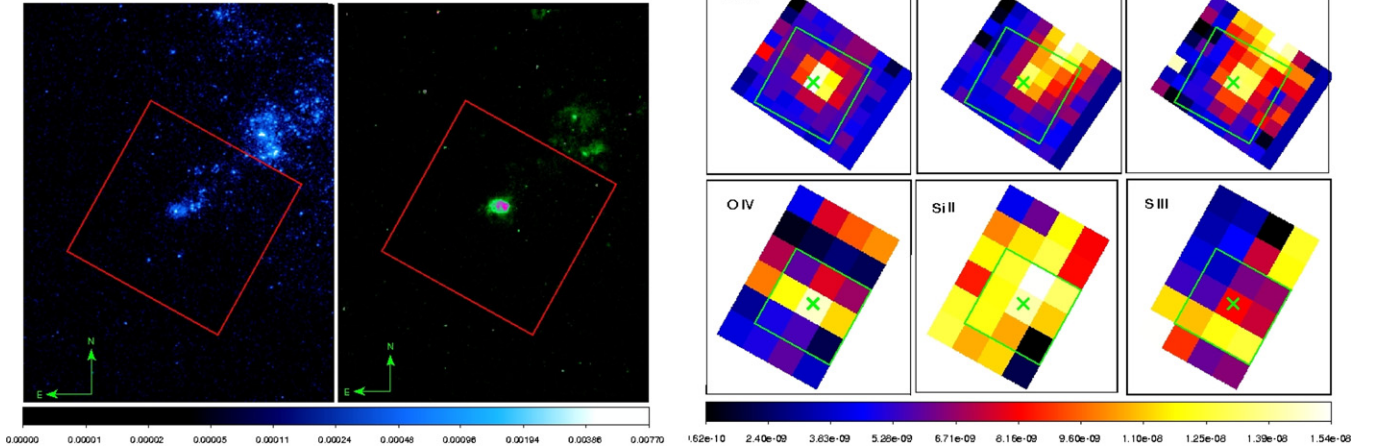
Figure 2. *HST* ACS images of the MF 16 nebula in NGC 6946 (left), and the *Spitzer* spectral maps of the infrared detected lines (right). The *HST* images are UV F140PL filter on the left and Hα on the right. The aperture used to extract IRS spectra is overplotted on all images. An OB association of bright stars are seen on the UV image just outside the aperture box. The low-ionization lines are clearly contaminated by these stars. The associated H II region is seen on the Hα image. The spectral maps are [Ne III] 15.56 μm, [Ne II] 12.81 μm, [S III] 18.71 μm, [O IV] 25.89 μm, [S III] 33.48 μm, and [Si II] 34.82 μm. The ULX UV counterpart identified by Kaaret et al. (2010) has the appearance of a bright star in the *HST* image, close to the center of the MF 16 nebula, and its position is shown with a green × on the spectral maps.

Table 1
Measured Infrared Lines

Line (1)	Flux (2)	S/N Ratio (3)	L (4)
[Ne II] 12.81 μm	2.5 ± 0.3	13.5	7.9 ± 0.9
Ne V 14.32 μm	<0.5	. . .	<1.5
Ne III 15.56 μm	2.3 ± 0.2	18.9	7.1 ± 0.7
S III 18.71 μm	1.3 ± 0.2	12.5	4.1 ± 0.7
Ne V 24.32 μm	<2.1	. . .	<6.7
O IV 25.89 μm	1.9 ± 0.2	12.8	6.0 ± 0.5
Fe II 25.99 μm	<1.2	. . .	<3.7
S III 33.48 μm	3.0 ± 0.2	24.3	9.4 ± 0.6
Si II 34.82 μm	2.4 ± 0.4	9.90	7.4 ± 1.4

Notes. Fluxes are in 10^{-21} W cm^{-2} and luminosities (L) are in 10^{37} erg s^{-1}. If the measurement errors are smaller than the absolute calibration accuracy of 25%, the latter were used. For non-detections we show 3σ upper limits.

the MF 16 nebula in UV and Hα emission. A nearby (200 pc away) star-forming region and the associated H II region can be seen just outside the *Spitzer* aperture. As can be seen in the *Spitzer* spectral maps, the low-ionization lines ([Ne II], [S III], and [Si II]) are contaminated by the surrounding star-forming region. In contrast, the higher ionization lines [O IV] and [Ne III] are clearly concentrated at the NGC 6946 X-1 location, suggesting a source of high-energy photons.

2.2. Archival Data

2.2.1. X-Ray Spectrum

We use X-ray spectroscopy in conjunction with published optical/UV data to model the X-ray emission from the ULX and to extract the full optical to X-ray spectrum. We also use it to estimate the UV emission by extrapolating the model to lower energies. To model the X-ray spectrum we used the best available data from the longest (∼58 ks) *Chandra* observation in the archive (ObsID 1043, taken on 2001 September 7). The data were processed by Berghea et al. (2008; U45 in this paper) and the spectrum is plotted in Figure 3.

We note that Fridriksson et al. (2008) find long-term X-ray flux variability of at most 30% in NGC 6946 X-1 based on *Chandra*, *XMM-Newton*, and *ROSAT* data. However, for completeness we have chosen the best data available to represent the source (e.g., *Chandra* data rather than *ROSAT* data), as well as one in which the luminosity is approximately averaged over the 10 years of observations (i.e., the 2001 data set). This average X-ray spectrum and luminosity best represents the ULX in a state in which the IR-line fluxes can be modeled. In addition, the equilibrium time-based recombination for the high-ionization lines is approximately 3000–100 years for He II and [O IV], respectively—well above the variability timescales of the X-ray source (Berghea et al. 2010b).

2.2.2. HST UV and Optical Photometry

We use the measurements obtained by Kaaret et al. (2010) to constrain the optical and UV emission from the accreting source and its companion. The *B*, *V*, *I*, and UV (F140LP filter) extinction-corrected fluxes are plotted as circles in Figure 3.

3. CLOUDY MODELING

3.1. Fitting the X-Ray Spectrum and Optical Data

We used XSPEC version 12.4 to model the spectrum between 0.3 and 8.0 keV. The X-ray spectrum is the most important component of the total SED since it is likely the only observed emission that directly emanates from the ULX and is not contaminated by the surrounding star-forming region. For this reason we have taken many precautions in modeling the X-ray spectrum, however, we fit the X-ray and optical/UV literature data simultaneously. In this section, we describe the models we chose to fit the X-ray spectrum and extrapolate to the unknown UV region not covered by literature data.

Probably the most common and simplest model for ULX X-ray spectra is the two-component model with a multi-color accretion disk component (MCD; Mitsuda et al. 1984) and a power law for the hard tail. However, this model cannot be extrapolated to UV where the source of IR lines originates (e.g.,
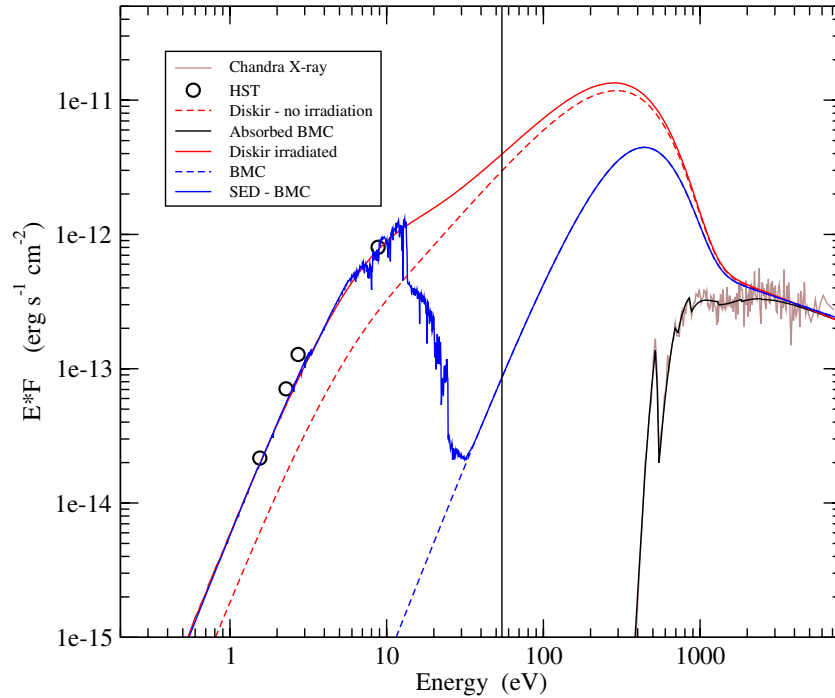
Figure 3. This figure shows the SED constructed in Section 3. The *Hubble* optical and UV data are quoted from Kaaret et al. (2010). The base model selected as the best fit from the Cloudy simulation (blue) is based on the BMC model fit to the X-ray data and a O9 I supergiant TLUSTY model star. We also show a model based on the DISKIR model (continuous red line). This includes irradiation of the outer disk replacing the companion (the disk without irradiation is shown with a dashed red line). The [O IV] edge at 54.93 eV is shown as a vertical line.

Done & Kubota 2006), and therefore we use the physically motivated Comptonization models described in detail below.

For all models, following Berghea et al. (2008), the Galactic absorption column density was fixed at 2.02×10^{21} cm^{-2}, and an additional local absorption ($N_{\rm H}$) model was added. We assume that the metallicity is approximately solar (see García-Benito et al. 2010 and references therein).

DISKIR model. The DISKIR model in XSPEC is a particularly useful Comptonization model to fit both optical and X-ray data because it also includes emission from an irradiated disk (Gierliński et al. 2009). We found that the best-fit model has a disk of radius 500 $R_{\rm in}$ (the inner disk radius), and the irradiated flux is at 1.5% of the total flux. The fraction of the flux thermalized in the inner disk was fixed at 0.1. In addition, the electron temperature kT_e and the radius of the Compton illuminated disk $r_{\rm irr}$ were set at 100 keV and 1.1, respectively. These values are typical for this model (e.g., Gierliński et al. 2009, 2008; Grisé et al. 2012).

BMC model. We also used the Bulk Motion Comptonization model (BMC in XSPEC) described by Titarchuk et al. (1997). Gliozzi et al. (2011) have suggested that this model is useful for ULX-like BH accretion scenarios. The best fit is obtained for a fraction of Comptonized flux of 0.12%.

SIRF model. Finally we tried the Self-IrRadiated Funnel model (SIRF in XSPEC), which describes the emission from a "supercritical funnel" (Abolmasov et al. 2009). This is created in objects similar to SS 433, by the wind formed at high accretion rates. Abolmasov et al. (2009) obtained a reasonable fit for *XMM-Newton* data of NGC 6946 X-1. The funnel opening angle was fixed at 20°, the inclination angle was set to zero, and the accretion rate fixed at an Eddington ratio of 10^4. These model parameters were set based on the best-fit results to the X-ray data. We obtained similar results for inner temperature and radius as Abolmasov et al. (2009), but unfortunately could

Table 2
X-Ray Model Fits

Model (1)	$N_{\rm H}$ (2) (10^{21} cm^{-3})	kT_{in} (3) (keV)	Γ/R_{in} (4)	$\Delta\chi^2$/dof (5)	L (6) (10^{40} erg s^{-1})
DISKIR	4.26 ± 0.11	0.118 ± 0.003	2.44 ± 0.08	1.16/183	7.01
BMC	$3.32^{+0.69}_{-0.39}$	0.110 ± 0.008	$2.40^{+0.08}_{-0.10}$	1.17/182	2.12
SIRF	$1.63^{+0.12}_{-0.08}$	$1.45^{+0.32}_{-0.11}$	$7.89^{+10.9}_{-3.8}$	1.85/182	1.39

Notes. Column 1: X-ray model, as described in Section 3.1; Column 2: intrinsic hydrogen column density. The Galactic column density from Berghea et al. (2008; 2.02×10^{21} cm^{-2}) was added separately; Column 3: inner disk temperature; Column 4: photon index for DISKIR and BMC models and the inner radius in 10^{-4} "spherization radius" units for the SIRF model (see Abolmasov et al. 2009); Column 5: reduced χ^2 values for the fit and the number of degrees of freedom; Column 6: unabsorbed (intrinsic) luminosities between 0.1 and 10 keV.

not find an acceptable fit using this model as Table 2 shows. As a result, this model has been disregarded as a viable model to fit the NGC 6946 X-1 SED in the discussion that follows.

The results from the X-ray fits are presented in Table 2, and the models are plotted in Figure 3. The first two models, DISKIR and BMC, both provide equally good fits to the X-ray data and will be used to construct the input SED for the CLOUDY modeling. However, as seen in Figure 3, they predict very different UV and optical emission, and therefore should yield very different results in the photoionization simulations. The physical difference between these two models is that the BMC model requires a bright optical companion to fit the optical and UV data. As seen in Figure 3, the DISKIR model fits the optical and UV data equally well with a bright (supergiant) companion (dotted red line) or an irradiated disk with a less luminous companion (solid red line).
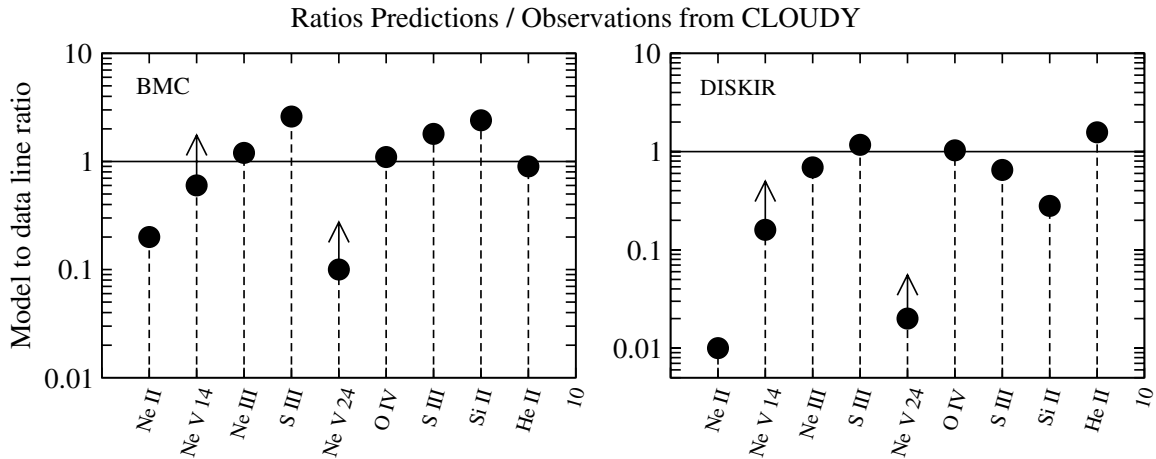
Ratios Predictions / Observations from CLOUDY

Figure 4. Line predictions from CLOUDY simulations. We show the results for both input models, BMC and DISKIR, as model-to-data flux ratios. The perfect match (ratio = 1) is shown as a horizontal line. Non-detections are marked with an arrow pointing upward.

Table 3
CLOUDY Modeling Results

Model	Radius	Depth	He II $\lambda4686$	[Ne II] 12.81	[Ne V] 14.32	[Ne III] 15.56	[S III] 18.71	[Ne V] 24.32	[O IV] 25.89	[Fe II] 25.99	[S III] 33.48	[Si II] 34.82
(1)	(2) (pc)	(3) (pc)	(4)	(5)	(6)	(7)	(8)	(9)	(10)	(11)	(12)	(13)
BMC	5.1	2.6	37.14	37.16	36.97	37.93	38.02	37.04	37.82	37.86	38.24	38.25
DISKIR	20.7	0.06	37.40	35.98	36.38	37.69	37.68	36.45	37.79	36.57	37.79	37.29

Notes. Column 1: SED model, as described in Section 3.1; Column 2: inner shell radius; Column 3: the thickness of the shell. Line luminosities are in units of log erg s^{-1}.

The model for the O9 I supergiant shown as the solid line in blue in Figure 3 is a TLUSTY (Hubeny & Lanz 1995) O star model with effective temperature 31,000 K, log g = 3.5, and a luminosity of 3.16×10^{39} erg s^{-1}. This fits the optical *HST* data (round black circles in Figure 3) very well. We add this star to both DISKIR and BMC models (dotted lines), but we remind our reader that the irradiated disk alone (solid red line) fits the optical–UV data equally well. Finally, we find that the SIRF model peaks just below the [O IV] edge, and is faint in the optical–UV, and therefore does not provide a good fit for these data as described above.

3.2. CLOUDY Photoionization Modeling

We use DISKIR and BMC SED models shown in Figure 3 as input spectra for CLOUDY. The bolometric luminosities that result from these models are 8.02 and 2.51×10^{40} erg s^{-1}, respectively. We assumed a solar metallicity as per García-Benito et al. (2010). Previous optical studies of NGC 6946 X-1 (Dunne et al. 2000; Blair et al. 2001; Abolmasov et al. 2008) indicate that the ionized gas from the nebula was swept inside a thin shell ($\sim$1 pc in width) around the ULX.

Estimates based on line ratios of [S II] suggest that the density of the gas in the shell is quite high (400–600 cm^{-3}; Blair et al. 2001; Abolmasov et al. 2008). If we use the ratio of the [S III] IR lines to estimate the density (Dudik et al. 2007), we obtain densities lower than 150 cm^{-3} for temperatures in the range 10,000–20,000 K (Abolmasov et al. 2008). However, Figure 2 shows that the [S III] lines are contaminated by the nearby star-forming region and therefore we prefer the higher value

obtained from previous optical line ratio estimates, since these were obtained from higher resolution maps. Thus, we assume a spherical shell geometry, a density of 400 cm^{-3}, and a filling factor of 0.2 (Blair et al. 2001).

The inner and outer radii of the shell were varied to obtain the best fit for the higher ionization lines [O IV] and [Ne III], since these IR lines are less contaminated by surrounding star-forming regions as illustrated in Figure 2. We also use the previously measured He II line flux (1.3×10^{37} erg s^{-1}) as a constraint (Wong 2010) since this line has an ionization potential similar to [O IV] and [Ne III] and likely emanates from a similar region to these IR lines. The predicted lines from the CLOUDY simulations are shown in Table 3 and Figure 4.

Previous optical observations have shown that radius of the shell (or shells) is 7–10 pc and the thickness is of the order of $\sim$1 pc (Blair et al. 2001). The DISKIR model is consistent with a shell of radius 20 pc and is thin compared to the findings of Blair et al. (2001) by a factor of $\sim$10. The BMC model predicts radial dimensions that are closer to those values observed by Blair et al. (2001), but the shell predicted is smaller by a factor of $\sim$1.5–2. A larger shell than Blair et al. (2001) is expected for the DISKIR model because it provides more ionizing photons. Both models are very good fits to the high-ionization IR lines as shown in Figure 4. However, the BMC model overpredicts most low-ionization lines, while DISKIR underpredicts them.

We finally note that both models underpredict the amount of gas compared to the Hydrogen column densities obtained from spectral fits. This could be explained if part of the absorption takes place very close to the accretion disk and not near the line-emitting region.

4. DISCUSSION

4.1. The Origin of the [O IV] Emission

Berghea et al. (2010b) discuss in detail possible scenarios for the [O IV] detected in the Holmberg II ULX in relation with AGNs and star-forming regions. The conclusions of that paper apply to NGC 6946 X-1 as well. The [O IV] is clearly associated with the ULX and not with the star formation nearby (Figure 2). Moreover, the hottest stars alone cannot produce the [O IV] measured from the MF 16 nebula. For more details we again direct our reader to Berghea et al. (2010b) and the references therein. An interesting result of that paper was that hot stars *can* have an important effect *if* a high-energy source is also present. The detailed CLOUDY simulation in Berghea et al. (2010b) showed that an O star can increase the [O IV] luminosity by a factor of three. This is also true in our case if the ULX companion is an O-star. We draw a similar conclusion based on the He II line, which has a very similar ionization potential to [O IV], and therefore requires a very high energy source.

The results of our CLOUDY modeling cannot easily discriminate between an O-star plus accretion disk and an irradiated disk (Figure 3). As discussed in Section 3.2, previous optical data suggest that the radius of the shell is 7–10 pc and the thickness is on order 1 pc (Blair et al. 2001). Table 3 shows that the BMC model predicts a radius and a thickness that are much closer to the optical findings than the DISKIR predictions. Finally, Figure 4 shows that the BMC model predictions for He II and [Ne III] are very slightly better than the DISKIR model predictions. For all of these reasons, we prefer the BMC model (the O-star plus accretion disk model) to the DISKIR model (an irradiated disk) to describe NGC 6946 X-1.

Berghea et al. (2010b) explored shocks as a possible mechanism for the lines for both NGC 6946 X-1 and Holmberg II ULXs. They found that the He II line is probably produced by shocks in the case of another famous nebula-surrounded ULX in Holmberg IX. However, for NGC 6946 X-1 and Holmberg II ULXs the He II emission is consistent with photoionization and not with shocks. To further confirm that the [O IV] alone is not dominated by shocks, we reproduced Figure 10(a) from Berghea et al. (2010b) for NGC 6946 X-1. We used the brightest pixel in the [O IV] spectral map to estimate a peak emission for this line. We note that this is in fact a lower limit for the estimate, since it represents the average flux over the large LH pixel. As shown in Figure 5, the shock velocity required to produce the peak [O IV] in NGC 6946 X-1 is in excess of 300 km s^{-1}. Dunne et al. (2000) find shock velocities from Hα are at most 270 km s^{-1}. This suggests that the shocks needed to produce the high-ionization lines [O IV] and He II are simply not present, based on the Hα data.

The ultimate source of X-ray and high-ionization emission in ULXs has been widely debated. Indeed, multiple mechanisms have been proposed to explain the high-energy emission, including beamed stellar-mass BHs, super-Eddington stellar-mass BHs, and finally, IMBHs. Evidence for one or more of these scenarios has been found for a variety of ULXs. While our observations and modeling of the ULXs in Holmberg II and the M16 nebulae strongly suggest these objects are not SNRs or beamed stellar-mass BHs, this analysis cannot distinguish between a super-Eddington stellar-mass BH or an IMBH as the source of the X-ray, optical, and high-ionization emission. This is due in part because the X-ray continuum is fit equally well with models describing either scenario. We note, on the
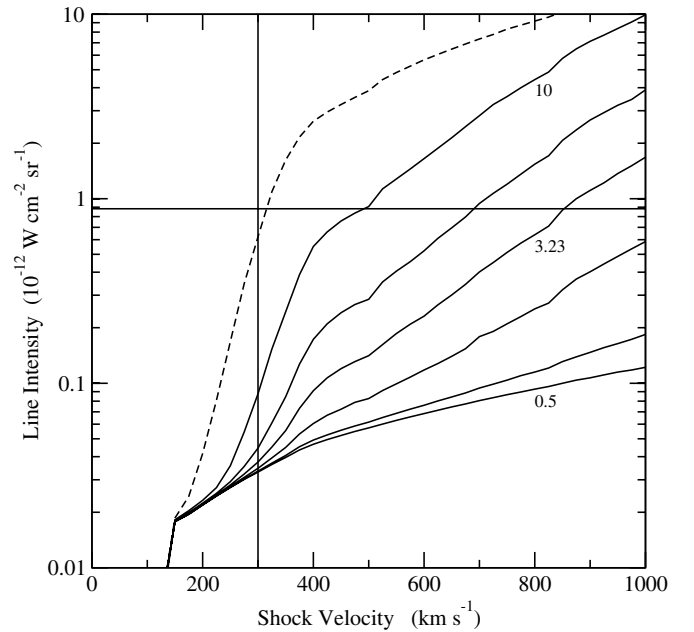

Figure 5. [O IV] line intensity shock predictions using Mappings III. The shocks plus precursor models vary little with the magnetic parameter, and we only show the model with a nominal equipartition value (3.23 μG cm$^{3/2}$; dashed line). The horizontal line corresponds to the brightest pixel in the [O IV] line map in Figure 2(b). The vertical line marks the higher limit of 300 km s^{-1} for shock velocities measured by Dunne et al. (2000).

other hand, that the infamous SS 433 in our Galaxy is a known beamed, super-Eddington stellar-mass BH with a clear host nebula. All evidence provided in the literature points to shocks or winds/outflows as the primary mechanism(s) for ionization in this object and the nebular region immediately surrounding the ULX (e.g., Abolmasov et al. 2010; Begelman et al. 1980, 2006). Because SS 433 is the only super-Eddington stellar-mass BH with a nebula definitively known to date, this is the only such source we have to compare with NGC 6946 X-1. Our analysis suggests that unlike SS 433, NGC 6946 X-1 has high-ionization lines (specifically the Oxygen line here and the He II from Abolmasov et al. 2008 that are most likely *not* produced by shocks). In this singular way the famous SS 433 super-Eddington stellar-mass BH is very different from NGC 6946 X-1.

The deficiency of super-Eddington sources in nebular environments precludes a detailed comparison of NGC 6946 X-1 with such objects. However, multiple active BHs in dense environments that produce high-ionization lines via photoionization are known to exist and are well documented in the literature. These sources, while not IMBHs, may prove an excellent comparative resource. For this reason, in the subsequent analysis, we focus attention on this comparison.

4.2. Diagnostic Line Ratios

The infrared [O IV] line (together with [Ne V]) is a signature of high ionization and excitation usually associated with actively accreting BHs (e.g., Lutz et al. 1998). This line is often used to disentangle the starburst emission in composite type galaxies and is a good indicator of the AGN power (Genzel et al. 1998; Sturm et al. 2002; Satyapal et al. 2004; Smith et al. 2004; Satyapal et al. 2007; Meléndez et al. 2008). Genzel et al. (1998) and Sturm et al. (2002) have used the ratio of [O IV]/[Ne II] to distinguish between starbursts and AGN-dominated galaxies
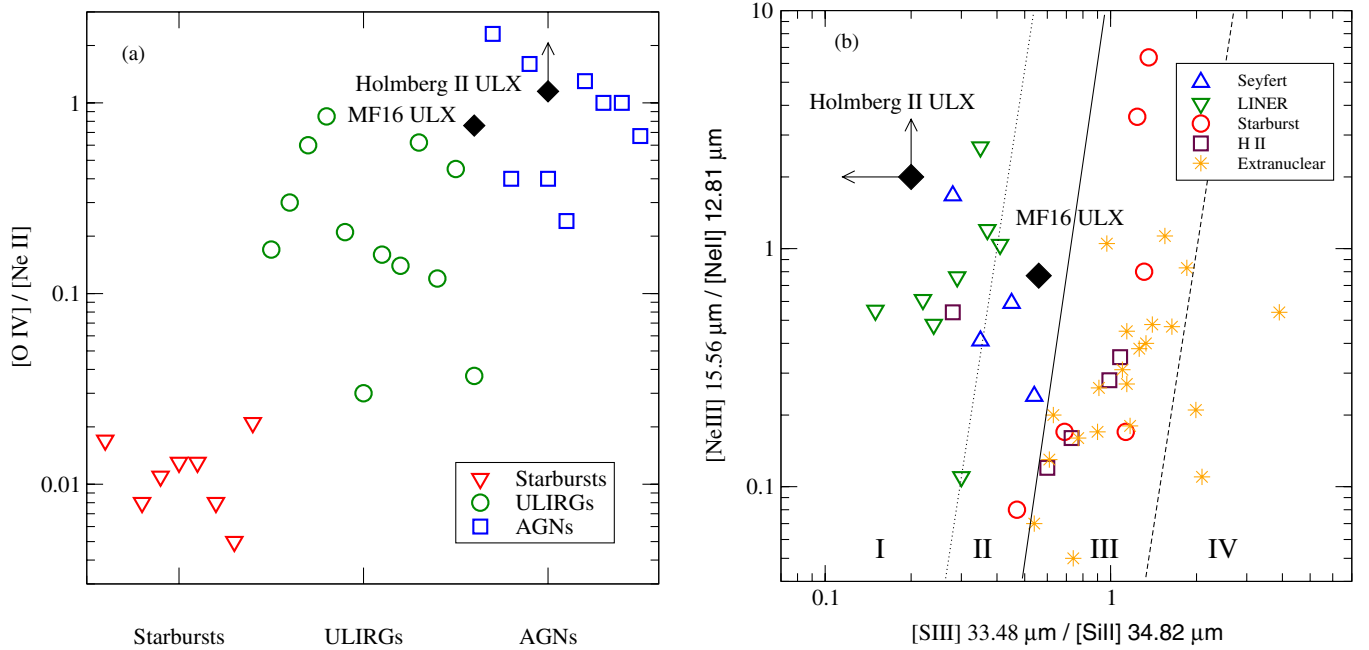
Figure 6. Ratio line diagnostics comparing the ULXs NGC 6946 X-1 and Holmberg II with other extragalactic ionizing sources: AGNs, starbursts, etc. Both plots suggest that the ULXs are very similar to AGNs and LINERs. (a) Diagnostic that uses the [O IV] line normalized to the [Ne II] line. The AGN, starburst, and ULIRG data are taken from Genzel et al. (1998). Many of the starbursts and ULIRGs are actually upper limits (see Figure 3 of Genzel et al. 1998). For Holmberg II ULX we show the lower limit because [Ne II] was not detected. (b) Diagnostic plot that uses the [S III] and [Si II] lines to distinguish between different sources. We plot all the data presented by Dale et al. (2006, their Figure 5), which includes: Seyferts, LINERs, starburst galaxies, H II regions, and extranuclear star-forming regions. For Holmberg II ULX we show the lower and upper limits because [Ne II] and [S III], respectively, were not detected.

in the mid-IR. In Figure 6(a), we compare the NGC 6946 X-1 mid-IR line ratios with data published by Genzel et al. (1998). The comparison clearly indicates high excitation for the ULX, similar to those seen in AGNs. The Holmberg II ULX from Berghea et al. (2010a) is also plotted here, though the [Ne II] flux for this ULX is an upper-limit. Both sources appear as AGN-like when this diagnostic is used.

Other infrared line diagnostics have been proposed by Dale et al. (2006, 2009) to disentangle AGN-type ionizing sources from star formation using the ratios [S III] 33.48 μm/[Si II] 34.82 μm and [Ne III]/[Ne II]. Figure 6(b) shows the four regions defined by Dale et al. (2006) from their Figure 5, and their published data for different sources in the SINGS sample. NGC 6946 X-1 is located well within region II, together with most Seyfert-like nuclei. Holmberg II is also plotted here from Berghea et al. (2010a) and shows ratios similar to low-luminosity nuclei, but we note that both [S III] and [Ne II] are upper limits for this object. We also note that the [S III], [Si II], and [Ne II] are heavily contaminated by star formation as is clear in the spectral maps in Figure 2. However, we also note that the AGN and star-forming regions presented by Dale et al. (2006, 2009) are subject to the same contamination biases and aperture effects as the ULXs. We therefore still find it useful to compare the two ULXs with these sources.

The fact that the Dale et al. (2006, 2009) ratios for NGC 6946 X-1 are Seyfert-like and that the [O IV]/[Ne II] ratio is quite high suggests that NGC 6946 X-1 is very gas rich compared to most ULXs and has a very strong UV source producing the ionizing radiation. We note that Vázquez et al. (2007) found similar results in their *Spitzer* IRS study of the NGC 4485/90 ULXs. However, they did not find clear evidence for [O IV] in their sample of objects. In examining this data further we find slightly discrepant ratios from Vázquez et al. (2007). From our analysis, only ULX-2 in their sample actually

falls marginally inside region I, the other five ULXs being located in regions II and III. In communicating with the authors we find that the discrepancy is likely due to differences in reduction pipeline used for processing or the apertures used in either analysis.

Finally, we compared the mid-IR line ratios for NGC 6946 X-1 (and Holmberg II ULX) with those of other objects presented in the diagnostic diagrams of Weaver et al. (2010). The error bars for the ULXs in this plot are approximately of the same size as the data points and represent 25% absolute calibration error for CUBISM (Smith et al. 2004). Weaver et al. (2010) find that high-ionization AGNs from the *Swift* Burst Alert Telescope (BAT) sample (Tueller et al. 2008, 2010) distinguish themselves from other less luminous AGNs and starburst galaxies in their [Ne III]/[Ne II] and [O IV]/[Ne II] ratios. A replication of the Weaver et al. (2010) plot is shown in Figure 7. These high-ionization AGNs have ratios very close to or over 1. In Figure 7, we overplotted the NGC 6946 X-1 as well as the Holmberg II ULX—the only two ULXs known to produce prominent [O IV] emission. Interestingly, NGC 6946 X-1 occupies the overlapping region between the high-ionization BAT AGNs and their lower-luminosity counterparts. The results for NGC 6946 X-1 are consistent with photoionization which is similar to that seen in low-ionization nuclear emission line region (LINER) or Seyfert-like nuclei rather than star forming in nature.

All three diagnostic diagrams suggest that the [O IV] emission in Holmberg II ULX and in NGC 6946 X-1 is dominated by the ULX and that the surrounding star-forming regions provide little contamination to this line. Both ULXs have been shown to be candidate IMBHs by other authors (Lehmann et al. 2005; Rao et al. 2010). While these findings cannot definitively prove that NGC 6946 X-1 is either an IMBH or a super-Eddington accretor, it does suggest that the environment may be very similar for this source and AGN-like objects. We finally mention that
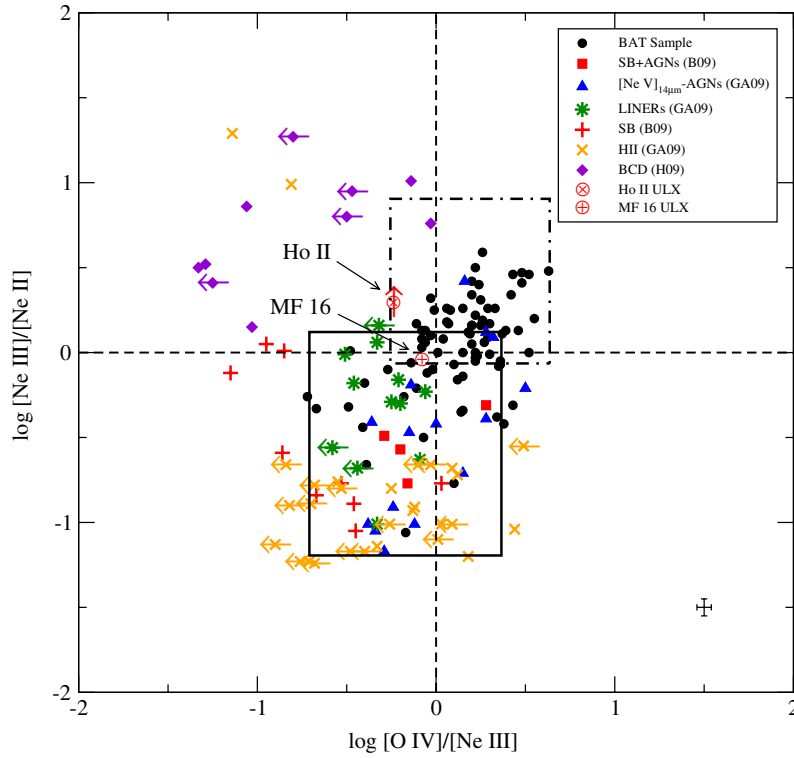
Figure 7. Line ratio diagnostics from Weaver et al. (2010). NGC 6946 X-1 line ratios clearly fit within the overlapping high-ionization and low-ionization AGN regime. This is only the second ULX to show such line ratios (see also Holmberg II).

the correlation of NGC 6946 X-1 with ultraluminous infrared galaxies (ULIRGs) in Figure 6(a) and LINERs in Figure 7 may lend some credence the predictions of McKernan et al. (2010, 2011) who suggest that many LINERs might host ULX-like IMBHs. Indeed many ULIRGs are LINERs (Satyapal et al. 2007; Dudik et al. 2007; Carrillo et al. 1999).

4.3. Black Hole Mass Estimates

Whether NGC 6946 X-1 is a super-Eddington source or an IMBH cannot be definitely determined from the observed and modeled data presented in this paper. However, as discussed in Section 4.2, the ratios from NGC 6946 X-1 look very similar to the ratios of well-known AGNs. We therefore find it useful to estimate the possible BH mass of this ULX based on AGN criteria with the caveat that the criteria assume NGC 6946 X-1 behaves much like an AGN which is not definitely known from the observed and modeled data presented here. The list below shows four BH mass estimates derived for NGC 6946 X-1.

1. Gliozzi et al. (2011, 2009) have proposed a new method to estimate BH masses using the BMC model. This method uses the photon index of the Comptonized part of the spectrum and the normalization to scale from well-known stellar-mass BHs with well-defined spectral transitions. Using a scaling method defined by Shaposhnikov & Titarchuk (2009) that is based on a detailed study of 8 different Galactic BH systems with 17 spectral transitions, Gliozzi et al. (2009, 2011) extend these scaling techniques to extragalactic BH sources. Indeed, one of these sources is a newly discovered ULX in NGC 3621. Thus, this technique can be used in the case of NGC 6946 X-1 as well, with the assumption that the states of ULXs mimic those of GBHB. It assumes that BHs of all masses show similar spectral states, at least with respect to Comptonization. If we scale the results from our BMC fits to XTEJ1550-564 (as done

by Gliozzi et al. 2011 in their Figure 1) and use $M_\odot = 9.1$ and $d = 4.4$ kpc from Orosz et al. (2011), and $\theta = 72$ from Gliozzi et al. (2011), we obtain a BH mass of $\approx 1800\ M_\odot$.

2. Both DISKIR and BMC X-ray models predict a cool disk. Assuming a BH accreting at the Eddington limit, the mass of the BH can be estimated at 1–$1.5 \times 10^4\ M_\odot$. However, this estimate assumes that the ULX is in a typical high state. If this is not the case, the inner disk temperature cannot be used reliably to estimate the mass of the BH (Stobbart et al. 2006).

3. Another estimate can be made just based on the bolometric luminosity calculated from our models. Using the values listed in Table 2, and assuming again accretion at Eddington limit, we obtain masses of 130 and 450 $M_\odot$.

4. Finally, Dasyra et al. (2008) found a good correlation between the luminosity of the [O IV] line and the mass of the central BH in standard AGNs. We estimate a BH mass of $2.7 \times 10^5\ M_\odot$ if this correlation is extrapolated to NGC 6946 X-1.

In conclusion these four methods predict a very wide range of BH masses for NGC 6946 X-1. Indeed the estimates predict masses that span three orders of magnitude: 10^2–$10^5\ M_\odot$, so emphasis on any one estimate is difficult to justify. However, it is interesting to note that all four put this object within the IMBH regime for the given criteria (e.g., accretion at the Eddington rate).

5. CONCLUSIONS

Using the mid-IR *Spitzer* spectral maps of NGC 6946 X-1 combined with *Chandra* X-ray and *HST* optical data from the literature, we model the SED of this unique ULX. We find the following major conclusions from our modeling and observational results.

1. The SED constructed based on X-ray and optical spectral modeling indicates that NGC 6946 X-1 is well fit with two Comptonization models: the DISKIR model and the BMC model, both available in XSPEC. Spectral modeling did not permit a good distinction between an irradiated disk or a bright companion plus accretion disk as source of the optical emission. However, the nebula parameters (namely radius and thickness) predicted by CLOUDY using the BMC model better match the findings from optical observations (Blair et al. 2001) and the lines are slightly better matched with the BMC model in this case. We therefore prefer the BMC model to the DISKIR model.

2. The detected [O IV] is consistent with photoionization by the strong X-ray emission from the ULX, and not with shocks or nearby star formation. This suggests that the X-ray emission is not strongly beamed. The data cannot, however, discriminate between super-Eddington accretion and the IMBH scenario.

3. We compared our results with known super-Eddington sources (i.e., SS 433) as well as standard AGNs. We find that the emission line properties of NGC 6946 X-1 are not well matched to the SS 433 super-Eddington source, since the lines from this source have been shown to be produced primarily by shocks. We also compared NGC 6946 X-1 line ratios with multiple AGN diagnostics. The line ratios from NGC 6946 X-1 consistently show emission very similar to most low-luminosity AGNs. We plotted diagnostic ratios from Genzel et al. (1998), Sturm et al. (2002), Dale et al. (2006), and Weaver et al. (2010). All plots show this ULX falling safely within the AGN regime rather than star-forming regions. This suggests that NGC 6946 X-1 may have photoionization and nebula properties that are similar to those seen in AGNs.

4. A variety of approximations were used to estimate the BH mass from the observed properties of this ULX and resulted in a predicted BH mass range spanning three orders of magnitude. Assuming this ULX is accreting at the Eddington limit we find that NGC 6946 X-1 has a BH mass between 10^2 and 10^5 $M_\odot$. Our calculations suggest that NGC 6946 X-1 could have a BH mass within the IMBH regime, with the caveat that the criteria for estimating BH mass assume NGC 6946 X-1 behaves much like an AGN which is not definitely known from the observed and modeled data presented here.

REFERENCES

Abolmasov, P. 2011, New Astron., 16, 138
Abolmasov, P., Fabrika, S., Sholukhova, O., & Afanasiev, V. 2007, Astrophys. Bull., 62, 36
Abolmasov, P., Fabrika, S., Sholukhova, O., & Kotani, T. 2008, arXiv:0809.0409
Abolmasov, P., Karpov, S., & Kotani, T. 2009, PASJ, 61, 213
Abolmasov, P., Maryeva, O., & Burenkov, A. N. 2010, Astron. Nachr., 331, 412
Begelman, M. C., Hatchett, S. P., McKee, C. F., Sarazin, C. L., & Arons, J. 1980, ApJ, 238, 722
Begelman, M. C., King, A. R., & Pringle, J. E. 2006, MNRAS, 370, 399
Berghea, C. T., Dudik, R. P., Weaver, K. A., & Kallman, T. R. 2010a, ApJ, 708, 354
Berghea, C. T., Dudik, R. P., Weaver, K. A., & Kallman, T. R. 2010b, ApJ, 708, 364
Berghea, C. T., Weaver, K. A., Colbert, E. J. M., & Roberts, T. P. 2008, ApJ, 687, 471
Blair, W. P., Fesen, R. A., & Schlegel, E. M. 2001, AJ, 121, 1497
Carrillo, R., Masegosa, J., Dultzin-Hacyan, D., & Ordoñez, R. 1999, RevMexAA, 35, 187
Colbert, E. J. M., & Mushotzky, R. F. 1999, ApJ, 519, 89
Cseh, D., Corbel, S., Kaaret, P., et al. 2012, ApJ, 749, 17
Dale, D. A., Smith, J. D. T., Armus, L., et al. 2006, ApJ, 646, 161
Dale, D. A., Smith, J. D. T., Schlawin, E. A., et al. 2009, ApJ, 693, 1821
Dasyra, K. M., Ho, L. C., Armus, L., et al. 2008, ApJ, 674, L9
Done, C., & Kubota, A. 2006, MNRAS, 371, 1216
Draine, B. T. 1989, in Infrared Spectroscopy in Astronomy (ESA SP-290), ed. B. H. Kaldeich (Noordwijk: ESA), 93
Dubner, G. M., Holdaway, M., Goss, W. M., & Mirabel, I. F. 1998, AJ, 116, 1842
Dudik, R. P., Weingartner, J. C., Satyapal, S., et al. 2007, ApJ, 664, 71
Dunne, B. C., Gruendl, R. A., & Chu, Y.-H. 2000, AJ, 119, 1172
Fabrika, S. 2004, Astrophys. Space Phys. Rev., 12, 1
Fender, R., & Belloni, T. 2004, ARA&A, 42, 317
Fridriksson, J. K., Homan, J., Lewin, W. H. G., Kong, A. K. H., & Pooley, D. 2008, ApJS, 177, 465
García-Benito, R., Díaz, A., Hägele, G. F., et al. 2010, MNRAS, 408, 2234
Genzel, R., Lutz, D., Sturm, E., et al. 1998, ApJ, 498, 579
Gierliński, M., Done, C., & Page, K. 2008, MNRAS, 388, 753
Gierliński, M., Done, C., & Page, K. 2009, MNRAS, 392, 1106
Gliozzi, M., Satyapal, S., Eracleous, M., Titarchuk, L., & Cheung, C. C. 2009, ApJ, 700, 1759
Gliozzi, M., Titarchuk, L., Satyapal, S., Price, D., & Jang, I. 2011, ApJ, 735, 16
Grisé, F., Kaaret, P., Corbel, S., et al. 2012, ApJ, 745, 123
Higdon, S. J. U., Devost, D., Higdon, J. L., et al. 2004, PASP, 116, 975
Hubeny, I., & Lanz, T. 1995, ApJ, 439, 875
Kaaret, P., & Corbel, S. 2009, ApJ, 697, 950
Kaaret, P., Feng, H., Wong, D. S., & Tao, L. 2010, ApJ, 714, L167
Kaaret, P., Ward, M., & Zezas, A. 2004, MNRAS, 351, L83
Kennicutt, R. C., Armus, L., Bendo, G., et al. 2003, PASP, 115, 928
King, A. R. 2008, MNRAS, 385, L113
Körding, E., Falcke, H., & Markoff, S. 2002, A&A, 382, L13
Kuncic, Z., Soria, R., Hung, C. K., Freeland, M. C., & Bicknell, G. V. 2007, in IAU Symp. 238, Black Holes from Stars to Galaxies—Across the Range of Masses, ed. V. Karas & G. Matt (Cambridge: Cambridge Univ. Press), 247
Lehmann, I., Becker, T., Fabrika, S., et al. 2005, A&A, 431, 847
Lutz, D., Kunze, D., Spoon, H. W. W., & Thornley, M. D. 1998, A&A, 333, L75
Matonick, D. M., & Fesen, R. A. 1997, ApJS, 112, 49
McKernan, B., Ford, K. E. S., & Reynolds, C. S. 2010, MNRAS, 407, 2399
McKernan, B., Ford, K. E. S., Yaqoob, T., & Winter, L. M. 2011, MNRAS, 413, L24
Meléndez, M., Kraemer, S. B., Schmitt, H. R., et al. 2008, ApJ, 689, 95
Miller, N. A., Mushotzky, R. F., & Neff, S. G. 2005, ApJ, 623, L109
Mitsuda, K., Inoue, H., Koyama, K., et al. 1984, PASJ, 36, 741
Moon, D.-S., Harrison, F. A., Cenko, S. B., & Shariff, J. A. 2011, ApJ, 731, L32
Orosz, J. A., Steiner, J. F., McClintock, J. E., et al. 2011, ApJ, 730, 75
Pakull, M., & Mirioni, L. 2002, in New Visions of the X-ray Universe in the XMM-Newton and Chandra Era (Noordwijk: ESTEC), (arXiv:astro-ph/0202488)
Pakull, M. W., Soria, R., & Motch, C. 2010, Nature, 466, 209
Poutanen, J., Lipunova, G., Fabrika, S., Butkevich, A. G., & Abolmasov, P. 2007, MNRAS, 377, 1187
Rao, F., Feng, H., & Kaaret, P. 2010, ApJ, 722, 620
Revnivtsev, M., Sunyaev, R., Gilfanov, M., & Churazov, E. 2002, A&A, 385, 904
Roberts, T. P., & Colbert, E. J. M. 2003, MNRAS, 341, L49
Satyapal, S., Sambruna, R. M., & Dudik, R. P. 2004, A&A, 414, 825
Satyapal, S., Vega, D., Heckman, T., O'Halloran, B., & Dudik, R. 2007, ApJ, 663, L9
Shaposhnikov, N., & Titarchuk, L. 2009, ApJ, 699, 453
Smith, J. D. T., Armus, L., Dale, D. A., et al. 2007, PASP, 119, 1133

Smith, J. D. T., Dale, D. A., Armus, L., et al. 2004, ApJS, 154, 199
Soria, R., & Kuncic, Z. 2008, in AIP Conf. Proc. 1053, Observational Evidence for Black Holes in the Universe, ed. S. K. Chakrabarti & A. S. Majumdar (Melville, NY: AIP), 103
Soria, R., Pakull, M. W., Broderick, J. W., Corbel, S., & Motch, C. 2010, MNRAS, 409, 541
Stephenson, C. B., & Sanduleak, N. 1977, ApJS, 33, 459
Stobbart, A-M., Roberts, T. P., & Wilms, J. 2006, MNRAS, 368, 397
Sturm, E., Lutz, D., Verma, A., et al. 2002, A&A, 393, 821
Titarchuk, L., Mastichiadis, A., & Kylafis, N. D. 1997, ApJ, 487, 834
Tueller, J., Baumgartner, W. H., Markwardt, C. B., et al. 2010, ApJS, 186, 378
Tueller, J., Mushotzky, R. F., Barthelmy, S., et al. 2008, ApJ, 681, 113
van Dyk, S. D., Sramek, R. A., Weiler, K. W., Hyman, S. D., & Virden, R. E. 1994, ApJ, 425, L77
Vázquez, G. A., Hornschemeier, A. E., Colbert, E., et al. 2007, ApJ, 658, L21
Weaver, K. A., Meléndez, M., Mushotzky, R. F., et al. 2010, ApJ, 716, 1151
Wong, S. W., Kaaret, P., & Feng, H. 2010, in JAXA Proc. of "The Energetic COSMOS: From Suzaku to ASTRO-H,", http://www-utheal.phys.s.u-tokyo.ac.jp/SuzakuConference2009/ProceedingsHTML/